2006

Theoretical Analysis of a Novel Rotary Compressor

Miguel E. Jovane
Purdue University

James E. Braun
Purdue University

Eckhard A. Groll
Purdue University

Seungun Lee
LG Electronics

THEORETICAL ANALYSIS OF A NOVEL ROTARY COMPRESSOR

Miguel E. Jovane[1]*, James E. Braun[1], Eckhard A. Groll[1], Seungjun Lee[2]

[1] Ray W. Herrick Laboratories
Purdue University
West Lafayette, Indiana 47907, USA
[2] DAC Laboratory,
LG Electronics,
391-2,Gaeumjeong-dong,Changwon City,Gyeongnam,641-711,Korea

*corresponding author: jovane@purdue.edu

ABSTRACT

A novel rotary compressor, termed the z-compressor, has been developed and is analyzed in this paper. The compressor has two chambers and performs two compression processes per rotation. The sequence in which the two compression processes are performed is similar to that of a twin rolling piston rotary compressor, although the geometry of this compressor is quite different. This novel compressor has the lowest noise and vibration operation compared to existing compressors. In this work, the characteristics of this compressor are presented and an analytical model that has been developed to study the performance of the z-compressor is described. The dimensions of the compressor, the suction pressure and temperature, and the discharge pressure are the input parameters of the model. Sample results generated with the model using refrigerant R410A as the working fluid are also presented in this work. These results focus on the impact of the leakage and frictional losses on the overall compressor performance.

1. INTRODUCTION

This paper presents a novel compressor that is within the family of rotary compressors. First, the geometry of the compressor is explained and equations relating the volume of the compression and suction chambers to the rotational angle of the shaft are derived. These equations are used within a model that predicts the mass flow rate and power consumption for the compressor. The model includes energy and mass balances within the compression chambers, as well as the estimation of leakage, frictional, and electrical losses. The primary sources of energy and flow losses are identified for this type of compressor. The presented results were generated using refrigerant R410a as the working fluid.

2. COMPRESSOR DESCRIPTION AND VOLUMETRIC CHARACTERISTICS

Similar to many rotary compressors, the z-compressor has a high pressure shell, and the refrigerant is brought into the suction chambers of the compressor by a tube. Figure 1 shows a CAD representation of the compressor without the shell. Similar to a twin rolling piston rotary compressor, the z-compressor performs two compression processes in one rotation. It is divided into upper suction and compression chambers and lower suction and compression chambers as seen in the cutaway view shown in Figure 2. The z-blade is one of the most innovative features of this compressor. The z-blade allows for volume variations as the shaft rotates without any eccentric rotation as occurs in the rolling piston rotary compressor. The upper and lower vanes provide separation between the suction and compression chambers of each level (upper and lower). The length of the portion of the vane affecting the volume of the chambers is dictated by the height of the portion of the z-blade in contact with the vane. This height, denoted y, is a function of the maximum height of the z-blade (h_b) and the rotation angle (θ) as follows,

$$y_u = \frac{h_b}{2}\left[1-\cos(\theta)\right] \tag{1}$$

$$y_l = \frac{h_b}{2}\left[1+\cos(\theta)\right] \tag{2}$$

where the subscripts u and l refer to the upper and lower level respectively, and the rotation angle (θ) is measured from the point of contact between the z-blade and the vane to the point at which the z-blade has zero height with respect to the upper level.. Equations (1) and (2) are used to estimate the volume of the chambers of the compressor as a function of the rotation angle.

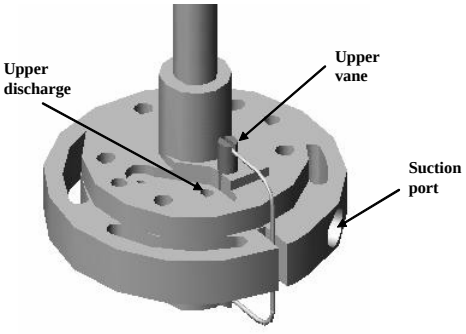

Figure 1: Schematic of the z-compressor

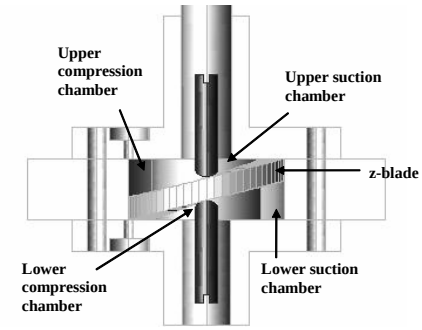

Figure 2: Cutaway view of the z-compressor

2.1 Volumetric characteristics

Integrating a differential volume element in cylindrical coordinates, the volume of the suction and compression chambers of the upper level are given by,

$$V_{s,u}(\theta) = \frac{V_{\max}}{2\pi}(\theta - \sin\theta) - \frac{V_{u,v}(\theta)}{2} \tag{3}$$

$$V_{s,u}(\theta) = \frac{V_{\max}}{2\pi}(2\pi - \theta + \sin\theta) - \frac{V_{u,v}(\theta)}{2} \tag{4}$$

where $V_{u,v}$ is the volume of the upper vane present inside the chambers, and V_{max} is the maximum chamber volume without the influence of the vane. V_{max} is given by

$$V_{\max} = \frac{\pi h_b\left(r_o^2 - r_i^2\right)}{2} \tag{5}$$

where r_i and r_o are the inner and outer radii of the z-blade. In deriving Equations (3) and (4) it has been assumed that one half of the volume of the vane present in the chambers affects the suction chamber while the other half affects the compression chamber. Similarly, the volume of the chambers corresponding to the lower level can be estimated using,

$$V_{s,l}(\theta) = \frac{V_{\max}}{2\pi}\left[\pm\pi + \theta - \sin(\theta \pm \pi)\right] - \frac{V_{l,v}(\theta)}{2} \tag{6}$$

$$V_{c,l}(\theta) = \frac{V_{\max}}{2\pi}\left[2\pi \mp \pi - \theta + \sin(\theta \pm \pi)\right] - \frac{V_{l,v}(\theta)}{2} \tag{7}$$

where the upper sign is used for angles smaller than π, and the lower sign for angles larger than π.

2.1.1. Vane volume

Early prototypes of the z-compressor as well as the current model were developed using a cylindrical vane. Figures 4 and 5 show the cylindrical vane and some important parameters related to the vane. Based on the parameters shown, the volume of the vane affecting the chambers of the upper and lower levels can be written as,

$$V_{v,u}(\theta) = \pi r_v^2 \left[y_u(\theta) - r_{nc} + \left(r_{nc}^2 - r_v^2 \right)^{1/2} \right] + V_{nc} \tag{8}$$

$$V_{v,l}(\theta) = \pi r_v^2 \left[y_l(\theta) - r_{nc} + \left(r_{nc}^2 - r_v^2 \right)^{1/2} \right] + V_{nc} \tag{9}$$

where, V_{nc} is the volume of the vane nose, and $y_l(\theta)$ is equal to $y_u(\theta)$ shifted by a half revolution. The volume of the vane nose can be estimated as,

$$V_{nc} = 2 \int_0^{\arcsin\left(\frac{r_v}{r_{nc}}\right)} \left(r_c^2 - \frac{r_c^2 - r_v^2}{\cos^2 \varphi} \right) \left[r_v^2 - \left(r_c^2 - r_v^2 \right) \tan^2 \varphi \right]^{1/2} d\varphi \tag{10}$$

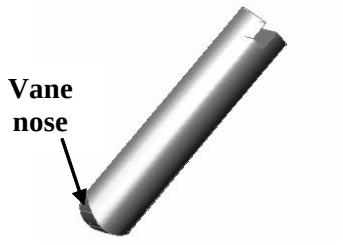

Figure 3: Cylindrical vane

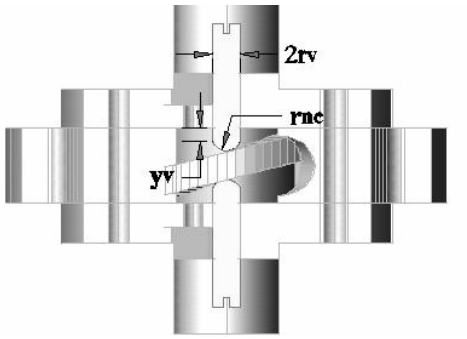

Figure 4: Cutaway view of the vane

With the knowledge of the relations for calculating the chamber volumes of the compressor and their variations with respect to the rotation angle, it is possible to start describing the model that has been developed to study the performance of the compressor.

3. MODEL DESCRIPTION

3.1. Mass and energy balance of the chambers of the compressor

A simplified system of conservation equations for the chambers of the compressor has been developed for the chambers of the upper level of the z-compressor. The upper and lower levels are assumed to behave exactly in the same way but shifted by a half revolution. In the simplified model, it is also assumed that the pressure in the suction chamber remains constant throughout the process. Heat transfer effects as well as the effect of the energy dissipated due to friction on the energy balance of the chambers are also neglected from the development of the system of conservation equations. Assuming quasi-equilibrium conditions and constant rotational speed, the transient mass and energy balance for the upper suction and compression chambers can be expressed as,

$$\begin{bmatrix} V_s \dfrac{\partial \rho_s}{\partial T} \dot{\theta} & -1 \\ V_s \dfrac{\partial (\rho u)_s}{\partial T} \dot{\theta} & h_s \end{bmatrix} \begin{bmatrix} \dfrac{dT_s}{d\theta} \\ \dot{m}_s \end{bmatrix} = \begin{bmatrix} -\rho_s \dfrac{dV_s}{d\theta} \dot{\theta} + \dot{m}_{l,net,s} \\ \sum \dot{m}_{l,s} h_{l,s} - (P_s + \rho_s u_s) \dfrac{dV_s}{d\theta} \dot{\theta} \end{bmatrix} \tag{11}$$

$$\begin{bmatrix} V_c \dfrac{\partial \rho_c}{\partial T} \dot{\theta} & V_c \dfrac{\partial \rho_c}{\partial P} \dot{\theta} \\ V_c \dfrac{\partial (\rho u)_c}{\partial T} \dot{\theta} & V_c \dfrac{\partial (\rho u)_c}{\partial P} \dot{\theta} \end{bmatrix} \begin{bmatrix} \dfrac{dT_c}{d\theta} \\ \dfrac{dP_c}{d\theta} \end{bmatrix} = \begin{bmatrix} -\rho_c \dfrac{dV_c}{d\theta} \dot{\theta} + \dot{m}_{l,net,c} + \dot{m}_d \\ \sum \dot{m}_{l,c} h_{l,c} - (P_c + \rho_c u_c) \dfrac{dV_s}{d\theta} \dot{\theta} + \dot{m}_d h_d \end{bmatrix} \tag{12}$$

For the suction chamber, the unknowns are the variations of the temperature inside the chamber, the mass flow rate through the suction port, and the leakage interactions with other chambers. For the compression chamber, the variations of temperature and pressure are unknown as well as the mass flow rate of discharged gas through the

discharge valve and the leakage interactions of the chamber. Note that all mass flow rates were assumed as entering the chamber. A negative sign should be added in those cases where the flow is leaving the chamber (e.g. discharge).

In order to solve the system of Equations (11) and (12), it was necessary to establish means to predict leakage interactions and the discharge mass flow rate. The relations used for these predictions are presented as follows.

3.1.1. Mass flow rate of leakage

For the z-compressor, nine leakage paths were identified. Figures 5 and 6 show the locations of these paths and the clearances associated with the leakage interactions.

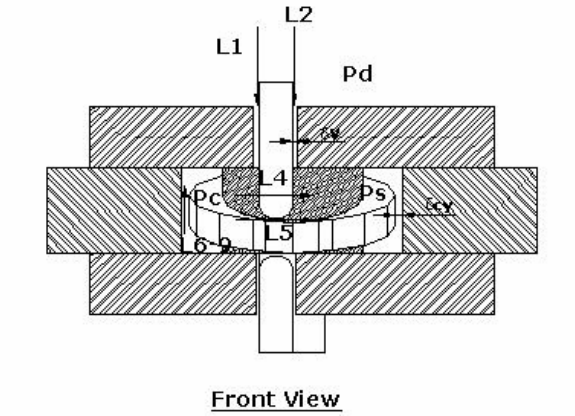

Figure 5: Leakage paths

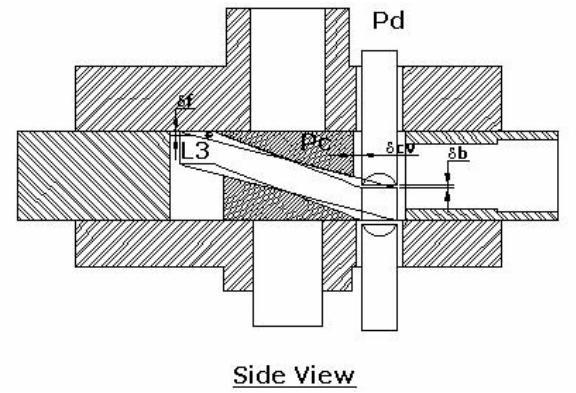

Figure 6: Leakage paths

As seen in Figure 5, mass leaks from the compression chamber to the suction chamber of its corresponding level, but there are also leakage paths that involve interactions between the chambers of the upper level with the chambers of the lower level. These are paths 6 through 9. Mass also leaks from the high pressure shell that is assumed to be at constant pressure and temperature. The interdependence between lower and upper levels suggests that the system of conservation equations for the upper level cannot be solved independently from the lower level. However, based on the assumption that the lower level passes through the same states with a half revolution shift, an iterative approach can be used. A set of pressures and temperatures can be assumed as initial guesses. These conditions are updated after each iterative simulation run.

The leakage paths of Figures 5 and 6 are exposed to different pressure ratios and have different lengths as summarized in Table 1.

Table 1: Leakage oath descriptions

Path	Description	Pressure Ratio	Area	Length [mm]
1	Leakage through the clearance of the bane and the bearing slot from the shell to the compression chamber	P_d:P_c	$0.5\pi\delta_v[r_v+(\delta_v/2)]$	15
2	Leakage through the clearance of the bane and the bearing slot from the shell to the suction chamber	P_d:P_s	$0.5\pi\delta_v[r_v+(\delta_v/2)]$	15
3	Leakage through the flat area of the blade	P_c:P_s	$0.5\delta_a[r_o-r_i]$	5.5
4	Leakage through the clearance of the vane and cylinder	P_c:P_s	$0.5\delta_{cv}y$	3.6
5	Leakage thought the clearance of the vane and the blade	P_c:P_s	$\delta_b r_v$	0
6	Leakage from the upper compression chamber to the lower suction chamber	$P_{c,u}$: $P_{s,l}$	$0.5\pi\delta_{cy}(r_o+\delta_{cy}/2)$ $\theta < 180^o$	7.2
7	Leakage from the lower compression chamber to the upper compression chamber	$P_{c,l}$: $P_{s,u}$	$0.5\pi\delta_{cy}(r_o+\delta_{cy}/2)$ $\theta > 180^o$	7.2
8	Leakage from the lower compression chamber to the upper suction chamber	$P_{c,l}$: $P_{s,u}$	$0.5(\pi-\theta)\delta_{cy}(r_o+\delta_{cy}/2)$ $\theta < 180^o$	7.2
9	Leakage from the upper compression chamber to the lower compression chamber	$P_{c,u}$: $P_{c,l}$	$0.5(2\pi-\theta)\delta_{cy}(r_o+\delta_{cy}/2)$ $\theta > 180^o$	7.2

As seen in Table 1, several leakage paths have lengths on the order of millimeters while the cross sectional areas are functions of the clearances, which are on the order of micrometers. For this reason, it was thought that friction effects along the leakage path should be considered. One option was to solve the system of mass, energy, and momentum equations along the leakage path, but this approach requires an iterative solution of a system of differential equations. As an alternative approach, a method where the stagnation pressure loss is predicted as a function of average properties is proposed. If the stagnation pressure at the exit of the path is known, isentropic relations can be used to predict the mass flow rate. A relation similar to that used to predict frictional pressure loss is proposed for this alternative approach as follows,

$$\Delta P_o = f \frac{\rho V^2 L}{D_H} \tag{13}$$

where f is a friction coefficient, ρ is the exit density, and V is the exit velocity. Once the stagnation pressure drop is determined, the mass flow rates are estimated using the following isentropic relations.

$$V = \left\{2\left[h_o\left(P_{o,e}, T_o\right) - h\left(s_{o,e}, P_b\right)\right]\right\}^{1/2} \tag{14}$$

or,

$$V = c\left(s_{o,e}, P > P_b\right) = \left\{2\left[h_o\left(P_o, T_o\right) - h\left(s_{o,e}, P\right)\right]\right\}^{1/2} \tag{15}$$

and,

$$\dot{m}_l = \rho V A \tag{16}$$

where, $s_{o,e} = s\left(T_o, P_{o,e}\right)$, and c is the speed of sound evaluated at the exit entropy. Equation (15) is used in a choked flow situation. It is observed that Equations (13) and (14) or (13) and (15) constitute a system of non-linear equations that need to be solved iteratively. Even though a number of iterations are required to solve the system, the computational effort is small compared to the effort required to solve the coupled mass, momentum, and energy equations along the leakage path.

3.1.2. Mass flow rate of discharge

The mass flow rate of discharge was estimated for those cases where the pressure in the compression chamber was greater than the pressure of the shell. An approach similar to the one developed to estimate the leakage mass flow rates was used. The opening area of the valve was calculated using a static force balance at the discharge port as was done by Chen et. al (2000). The opening area is then estimated by,

$$A = yD\pi \tag{17}$$

$$y = \pi\left(P_c - P_d\right)D^2 \big/ 4k_{valve} \tag{18}$$

where D is the diameter of the discharge port, and k is the elastic constant of the reed valve that was curve-fitted using a fourth order polynomial with y as the independent variable.

The friction coefficient in Equation (13) was considered constant. The coefficient was determined such that the average mass flow rate predicted using the model matched the mass flow rate of the compressor estimated by running the compressor at the same suction and discharge conditions.

3.2. Friction and motor losses

The mass and energy balances of the chambers of the compressor were coupled to a force analysis where the predicted pressure distribution was used to estimate the axial and radial loads that the thrust and journal bearings needed to overcome. Models for the bearings are used to calculate the frictional losses due to the relative motion of components. The radial load was carried by two journal bearings. The bearings were modeled using the long bearing assumption. The load carried by each bearing was decided using the criteria that the radial displacement of the shaft (eccentricity) was the same for both bearings. Based on the assumption of quasi-equilibrium conditions, steady-state relations were used to study the losses associated with the journal bearing. The thrust bearings were modeled as a squeeze damper where the changes in the film thickness due to the shaft displacement in the axial direction produce

the lubricant force necessary to balance the axial pressure force. Other sources of friction losses considered were the contact of the z-blade with the cylinder as well as the contact of the flat region of the blade and the bearings as shown in Figure 7. These last two sources of friction loses were model assuming Couette flow.

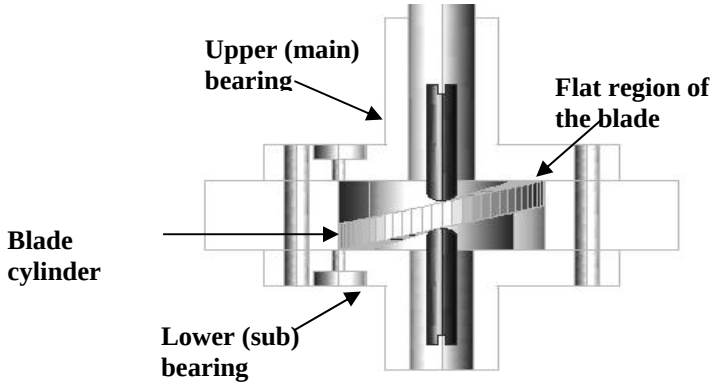

Figure 7: Sources of friction losses

The force analysis provided information on the shaft work required. With the shaft power requirement and by knowing the relation between the motor efficiency and the rotational speed, it is possible to estimate the power consumption of the motor which is the overall power consumed by the compressor. The difference between the shaft power and the motor power (electric losses) are used to perform a steady-state energy balance on the shell of the compressor. This energy balance provided the means to calculate the temperature of the refrigerant in the shell of the compressor, which is the temperature of the gas leaving the device and is also the temperature of the refrigerant leaking through paths 1 and 2. For this steady state analysis, the temperature of the refrigerant in the shell is assumed uniform. It is also assumed that the shell is able to exchange heat with the surrounding through natural convection. The wall temperatures of the shell were assumed equal to the temperature of the refrigerant.

The combined analysis (compression, friction, shell energy balance) was solved iteratively by first assuming a shell temperature as well as a pressure distribution. The guessed values were updated after each solution was obtained until the results did not change any more. The results of this analysis are summarized in the following section.

4. RESULTS AND DISCUSSION

The model developed and previously described was run using the geometric parameters shown in Tables 2 and 3, and the operating conditions shown in Table 4. The geometric parameters of Table 2 are tabulated as non-dimensional quantities relative to the radius of the shaft in contact with the upper bearing, and the clearances of Table 3 are also tabulated as non-dimensional quantities relative to the total axial clearance (δ_a). For the specified set of operating conditions, the predicted average mass flow rate and power consumption are 57 kg/h and 935.2 W respectively. The estimated power input was within 6% of the experimental point used to determine the friction coefficient for leakage losses and discharge mass flow rate. The volumetric efficiency at these conditions is 91% and the overall isentropic efficiency is 67.1%. This overall efficiency is comparable to the 64.3% and 67.2% that Sakaino et al. (1986) reported for single and dual cylinder rolling piston rotary compressors, respectively. It is important to point out that the results by Sakaino et al. were estimated for a 3.75 kW compressor and that the authors did not report the refrigerant used. However, based on the reported operating conditions, most likely the refrigerant R22 was used. The volumetric efficiencies reported by the authors were 95% for the single cylinder rolling piston compressor and 97.7% for the twin rolling piston compressor. These volumetric efficiencies are greater than the ones reported in this study. One reason for this difference is the greater pressure ratio that a compressor operating with refrigerant R410A needs to accomplish compared to the pressure ratio when R22 is used. This generates greater potential for leakage losses. As it is known, irreversibilities due to leakage can have a negative effect on the efficiency of the compressor. Figure 8 shows the average leakage losses for the nine paths described in Section 3.1. In generating these results, it was assumed that the contact between the vane and the blade was almost a metal to

metal contact and leakage through this contact (path 5) was neglected. It is observed from Figure 8 that the leakage paths 6 through 9, which represent the interactions between the upper and lower levels of the compressor, have the most significant magnitude. These four leakage paths have the largest flow area. The smallest contribution to leakage losses comes from the paths that represent interactions with the shell and the chambers (paths 1 and 2). For these paths, the flow area is small and also the leakage path has an approximated length of 15 mm. Since frictional effects were considered in predicting leakage loses, the length of the path is important in the stagnation pressure loss through the path. The longer the path, the larger the stagnation pressure loss and the smaller the mass flow rate of leakage.

Other important losses associated with the performance of the compressor are frictional losses. The average losses for the contacts where losses were estimated are presented in Figure 9. The mechanical efficiency of the compressor when accounting for these frictional losses is approximately 92%. It is observed that the frictional losses on the contact between the blade and cylinder are significant. However, leakage losses between the upper and lower chambers through the clearance between the blade and cylinder were also significant. Therefore, reducing the clearance between the blade and cylinder to reduce leakage losses is not a good option because it would increase frictional losses at the blade-cylinder contact. Another solution is the implementation of a piston ring around the blade to minimize leakage losses through the contact. The study of these options is out of the scope of this publication.

Table 2: Compressor dimensions

Component	Dimension
Shaft radius (Main bearing)	1.00
Shaft radius (Sub-bearing)	0.94
Blade inner radius (r_i)	2.15
Blade outer radius (r_o)	3.05
Maximum chamber height (h_b)	1.50
Vane radius (r_v)	0.45
Vane nose cap radius (r_{nc})	0.50
Main journal bearing length	6.00
Sub journal bearing length	4.13

Table 3: Clearances

Component	Clearance
Total axial clearance (δ_a)	1.00
Clearance of the vane and bearing slot (δ_v)	0.32
Clearance between the vane and cylinder (δ_{cv})	0.54
Clearance of the blade and cylinder contact (δ_{cy})	1.16
Clearance of the main journal bearing	0.48
Clearance of the sub journal bearing	0.68

Table 4: Operating conditions

Rotating speed [RPM]	2836
Suction temperature [K]	308.15
Suction pressure [kPa]	995.38
Discharge pressure [kPa]	3381.65

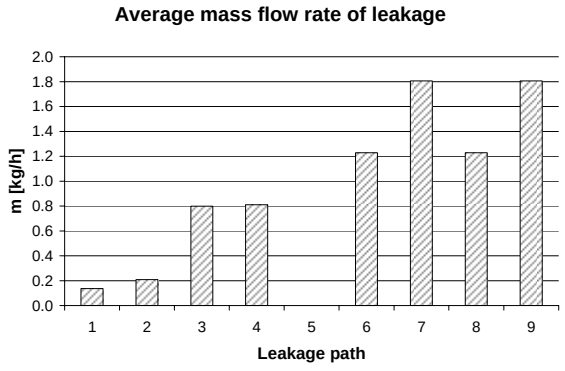

Figure 8. Average leakage losses

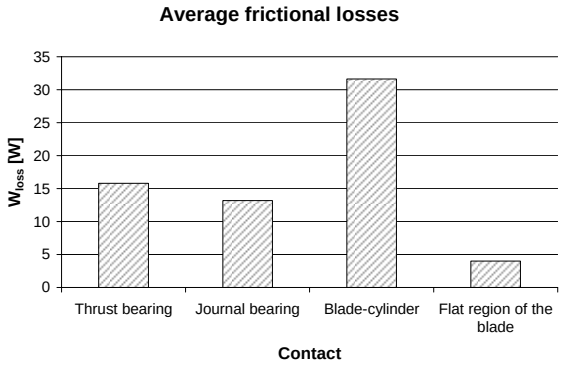

Figure 9. Average friction losses

5. CONCLUSIONS

A detailed analysis of a novel rotary compressor, called z-compressor, was performed to evaluate the overall performance of the compressor and to identify the main sources of leakage and frictional losses. The most significant leakage and frictional losses are related to the clearance between the blade and the cylinder. The analysis showed that the volumetric efficiency of the z-compressor is 91% and the overall isentropic efficiency is 67.1% at typical rating point conditions. Based on the presented results, there is potential for improving the efficiency of the compressor if the mass flow losses and friction losses in the contact area between the cylinder and the blade are reduced. This can be done in different ways such as installing a piston ring around the blade such that leakage losses are reduced. As previously mentioned, reducing the clearance of this contact would increase frictional losses while decreasing leakage losses, so there should be an optimum clearance. Additionally, these friction and leakage losses around the blade-cylinder contact can be reduced by reducing the outer radius of the blade. This would require an increase in the maximum chamber height which could have an increasing effect on the leakage losses through the vane. Therefore, an optimum ratio of the blade outer ratio and chamber height needs to be determined. Being able to optimize the efficiency of the compressor would add to the already low noise and vibration effects increasing the potential of this device.

ACKNOWLEDGEMENT

The authors would like to acknowledge the contributions to this work made by Dr. Samchul Ha, Vice President and Director of Digital Appliance Laboratory of LG Electronics, as well as the contribution of the DAC Laboratory of LG Electronics in Changwon, in particular the contribution by Kwanshik Cho, Youngju Bae, and the contribution of Dr. Byoung Ha Ahn (Air Conditioning Laboratory, LG Electronics).

NOMENCLATURE

A	Cross sectional area [m^2]
c	Sound speed [m/s]; clearance [m]
D_H	Hydraulic diameter [m]
f	Friction coefficient
h	Specific enthalpy [J/kg]; lubricant film thickness [m]; heat transfer coefficient [W/m^2]
h_b	Maximum chamber height [m]
h_c	Specific enthalpy of the refrigerant in the compression chamber [J/kg]
h_{in}	Specific enthalpy of the refrigerant entering through the suction port [J/kg]
$h_{l,c}$	Specific enthalpy of the refrigerant entering/leaving the compression chamber due to leakage [J/kg]
$h_{l,s}$	Specific enthalpy of the refrigerant entering the suction chamber due to leakage [J/kg]
h_o	Specific stagnation enthalpy [J/kg]
k_{valve}	Coefficient of elasticity of the valve [N/m]
L	Length of leakage path [m]
$\dot{m}_{1,2,...,n}$	Mass flow rate of leakage through the nth leakage path [kg/s]
$\dot{m}_d$	Mass flow rate leaving the compressor chamber through the discharge port [kg/s]
$\dot{m}_{l,net,c}$	Net mass flow rate of leakage associated with the compression chamber [kg/s]
$\dot{m}_{l,net,s}$	Net mass flow rate of leakage associated with the suction chamber [kg/s]
$\dot{m}_s$	Mass flow rate entering the through the suction port [kg/s]
P	Pressure [Pa]
P_b	Back pressure [Pa]
P_d	Discharge pressure [Pa]
P_o	Stagnation pressure [Pa]
r_i	Inner blade radius [m]
r_{nc}	Radius of the vane nose cap [m]
r_o	Outer blade radius [m]
r_s	Shaft radius [m]

r_v	Vane radius [m]
s_o	Stagnation entropy [J/kg-K]
T	Temperature [K]
t	Time [s]
T_d	Discharge temperature [K]
T_o	Stagnation temperature [K]
u	Specific internal energy [J]
V	Volume [m^3], velocity [m/s]
V_c	Volume of the compression chamber [m^3]
V_{max}	Maximum chamber volume [m^3]
V_{nc}	Volume of the vane nose cap [m^3]
V_s	Volume of the suction chamber [m^3]
V_v	Volume of the vane inside the chambers [m^3]
y	Chamber height, discharge valve lift; shaft displacement [m]

Greek letters

δ_a	Axial clearance [m]
δ_{cv}	Clearance between the vane and cylinder [m]
δ_{cy}	Clearance between the blade and cylinder [m]
δ_v	Clearance between the vane and bearing slot [m]
θ	Rotation angle [radians]
$\dot{\theta}$	Rotational speed [radians/s]
ρ	Density [kg/m^3]

Subscripts

c	Compression chamber
l	Lower chambers
s	Suction chamber
u	Upper chambers

REFERENCES

Chen, Y., Groll, E.A., Braun, J.E. 2000. *Mathematical Modeling of Scroll Compressor*. HL 2000-17P, Report #3147-1. Ray W. Herrick Laboratories. Purdue University.

Hamrock, B.J. 1994. *Fundamentals of Fluid Film Lubrication*. McGraw-Hill.

Hoffman, J.D., 1992. *Numerical Methods for Scientists and Engineers*. McGraww-Hill.

Hwang, S.W., Kim, K.H., Lee, S.Y., Kim, J.S., Park, S.K. 1998. *Development of High Efficiency Rolling Piston Type Rotary Compressor for Alternative Refrigerant R410a*. Purdue Compressor Technology Conferences. Purdue University.

Matsuzaka, T., Nagatomo, S. 1982. *Rolling Piston Type Rotary Compressor Performance Analysis*. Purdue Compressor Technology Conferences. Purdue University.

Pandeya, P.N., Soedel, W. 1978. *Rolling Piston Type Rotary Compressor with Special Attention to Friction and Leakage*. Purdue Compressor Technology Conferences. Purdue University.

Pinkus, Oscar and Sternlicht, Beno. 1961. *Theory of Hydrodynamic Lubrication*; McGraw-Hill.

Sakaino, K., Kawasaki, K., Shirafuji, Y., Ohinata, O. 1986. *The Study of Dual Cylinder Rotary Compressor*. Purdue Compressor Technology Conferences. Purdue University.

Soedel, W. 1984. *Design and Mechanics of Compressor Valves*. Ray W. Herrick Laboratories. Purdue University.

Wakabayashi, H., Yuuda, J., Aizawa, T., Yamamura, M. 1982. *Analysis of Performance in a Rotary Compressor*. Purdue Compressor Technology Conferences. Purdue University.

Zucrow, M., Hoffman, J.D. 1976. *Gas Dynamics Vol. 1*. McGraw-Hill